RECONSTRUCTING THE γ-RAY PHOTON OPTICAL DEPTH OF THE UNIVERSE TO $z \sim 4$ FROM MULTIWAVELENGTH GALAXY SURVEY DATA

Kari Helgason[1,2] and Alexander Kashlinsky[2,3]
[1] Department of Astronomy, University of Maryland, College Park, MD 20742, USA; kari@astro.umd.edu
[2] Observational Cosmology Laboratory, Code 665, NASA Goddard Space Flight Center, Greenbelt, MD 20771, USA
[3] SSAI, Lanham, MD 20706, USA; alexander.kashlinsky@nasa.gov

ABSTRACT

We reconstruct the γ-ray opacity of the universe out to $z \lesssim 3$–4 using an extensive library of 342 observed galaxy luminosity function (LF) surveys extending to high redshifts. We cover the whole range from UV to mid-IR (0.15–25 μm) providing for the first time a robust empirical calculation of the $\gamma\gamma$ optical depth out to several TeV. Here, we use the same database as Helgason et al. where the extragalactic background light was reconstructed from LFs out to 4.5 μm and was shown to recover observed galaxy counts to high accuracy. We extend our earlier library of LFs to 25 μm such that it covers the energy range of pair production with γ-rays (1) in the entire *Fermi*/LAT energy range, and (2) at higher TeV energies probed by ground-based Cherenkov telescopes. In the absence of significant contributions to the cosmic diffuse background from unknown populations, such as the putative Population III era sources, the universe appears to be largely transparent to γ-rays at all *Fermi*/LAT energies out to $z \sim 2$ whereas it becomes opaque to TeV photons already at $z \lesssim 0.2$ and reaching $\tau \sim 10$ at $z = 1$. Comparing with the currently available *Fermi*/LAT gamma-ray burst and blazar data shows that there is room for significant emissions originating in the first stars era.

Key words: cosmic background radiation – galaxies: evolution – gamma rays: general

Online-only material: color figures

1. INTRODUCTION

The extragalactic background light (EBL) supplies opacity for propagating high-energy GeV–TeV photons via an electron–positron pair production ($\gamma\gamma \rightarrow e^+e^-$) (Nikishov et al. 1962; Stecker 1971). Determining the transparency of the universe is of fundamental importance for a wide variety of current observatories such as the space-borne *Fermi*/LAT instrument operating at energies $\lesssim$250–300 GeV to ground-based γ-ray telescopes probing energies $\gtrsim$1 TeV. The distance at which the optical depth due to this interaction is $\tau \sim 1$ defines a horizon of the observable universe at γ-ray energies, and has been a subject of extensive efforts designed to model the buildup of EBL with time from the posited emission history of galaxy populations (e.g., Stecker et al. 2006; Franceschini et al. 2008; Kneiske & Dole 2010; Domínguez et al. 2011).

In this Letter, we show that, with observed galaxy populations over a wide range of wavelengths, one can uniquely reconstruct the optical depth of the universe at these energies out to redshifts $z \sim 4$. This empirical reconstruction relies exclusively on data from an extensive library of galaxy luminosity functions (LFs) encompassing 18 finely sampled wavelengths from UV to mid-IR (0.15–24 μm) relevant for the pair-production opacity. This methodology enables robust calculation of the γ-ray opacity in the *Fermi*/LAT energy range using galaxy surveys probing $\lambda \leqslant 4.5 \mu$m out to $z \lesssim 4$. Extending to TeV energies, probed by the ground-based Cherenkov observations, we use measurements out to 24 μm; this extrapolation is robust for the redshifts currently probed these observations. This heuristic reconstruction using the *observed* galaxy populations defines the absolute floor of the photon–photon optical depth due to known galaxy populations and deviations from it would allow the characterization of any emissions inaccessible to direct telescopic studies (Kashlinsky 2005b; Gilmore 2012).

We use the methodology developed in Helgason et al. (2012) of reconstructing the EBL from observed galaxy populations in a compilation of 342 measured LFs covering the UV, optical, and near-IR; that compilation is slightly updated compared to Table 1 of Helgason et al. (2012). The wealth of galaxy survey data has recently reached adequate redshift coverage to make such empirical estimation of the evolving EBL feasible and the reconstruction was shown to reproduce independent data from galaxy counts and the cosmic infrared background (CIB; Kashlinsky 2005a). Our approach is completely independent of theoretical modeling describing the evolution of galaxy populations in that we use the LF data directly observed at all wavelengths out to $z \sim 3$–8 in this heuristic reconstruction from which we derive the optical depth due to pair production. (see also Stecker et al. 2012).

Standard cosmological parameters are used below: $\Omega_{\rm tot} = 1$, $\Omega_{\rm m} = 0.3$, $H_0 = 70$ km s^{-1} Mpc^{-1}.

2. RECONSTRUCTING THE EVOLVING EBL FROM DATA

Quantifying the optical depth of the universe to high-energy photons requires knowledge of the properties of the intervening EBL. Evolving galaxy populations compose the bulk of the EBL, which is dominated by starlight in the UV/optical and thermally radiating dust at longer IR wavelengths. We use multiwavelength survey data to fit the evolution of a single derived quantity, the luminosity density, in this otherwise assumption-free approach. We cover the whole range from UV to mid-IR (0.15–25 μm), providing for the first time an empirical derivation of the $\gamma\gamma$ optical depth out to several TeV. Stecker et al. (2012) used a similar approach to reconstruct the EBL at $<0.7 \mu$m. The survey data used in this Letter extends the collection of LFs presented in Helgason et al. (2012) with expanded coverage in the UV (Steidel et al.
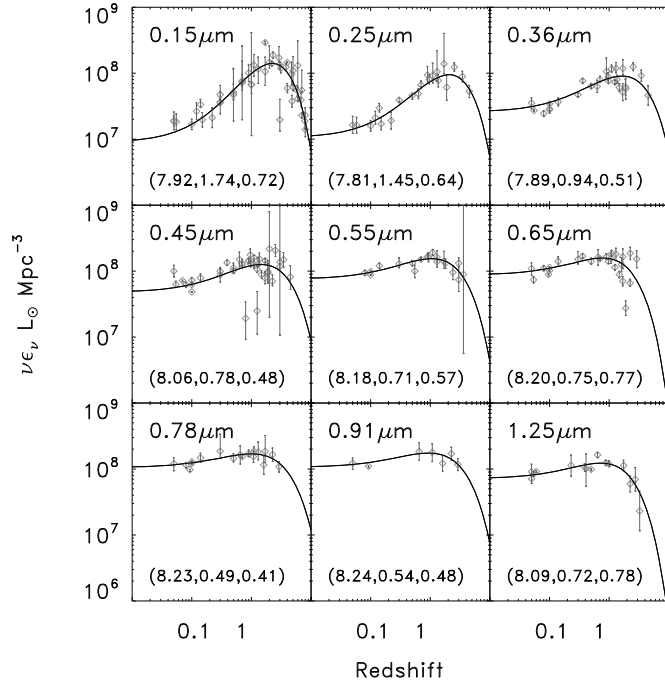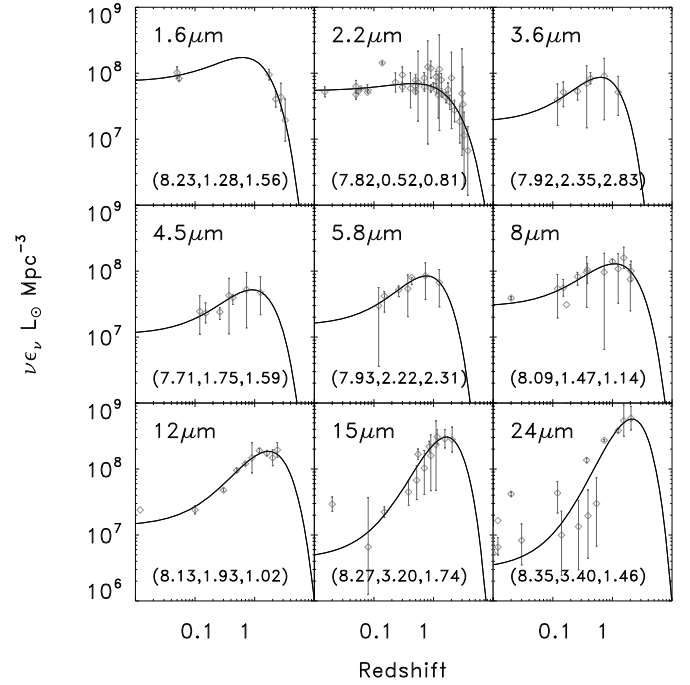
Figure 1. Measurements of the evolving luminosity density in our binned rest-frame wavelength range 0.14–1.25 μm in units of $L_\odot$ Mpc^{-3}. The solid curves are fits through the data points according to our fitting function (Equation (2)) with best-fit parameters displayed in each panel as ($\log_{10} a_\lambda, b_\lambda, c_\lambda$) where a_λ is also in $L_\odot$ Mpc^{-3}. All data points have been converted to units with $h = 0.7$. The references for the data points can be found in Table 1 of Helgason et al. (2012) with the addition of UV data from Steidel et al. (1999), Sullivan et al. (2000), Treyer et al. (2005), Schiminovich et al. (2005), Budavári et al. (2005), Sawicki & Thompson (2006), and Finkelstein et al. (2012).

Figure 2. Same as Figure 1 for infrared wavelengths, 1.6–24 μm. The references for the data points can be found in Table 1 of Helgason et al. (2012) with the addition of mid-IR data from Shupe et al. (1998), Xu et al. (1998), Sanders et al. (2003), Le Floc'h et al. (2005), Pérez-González et al. (2005), Rujopakarn et al. (2010), and Magnelli et al. (2011).

1999; Sullivan et al. 2000; Treyer et al. 2005; Schiminovich et al. 2005; Budavári et al. 2005; Sawicki & Thompson 2006; Tresse et al. 2007; Finkelstein et al. 2012) and out to mid-IR wavelengths (Rujopakarn et al. 2010; Shupe et al. 1998; Xu et al. 1998; Sanders et al. 2003; Le Floc'h et al. 2005; Magnelli et al. 2011; Pérez-González et al. 2005). This library now contains 342 measured LFs and allows us to reconstruct the evolving EBL and its spectrum in a finely sampled wavelength grid encompassing 0.15–24 μm out to $z \sim 2$–8. Helgason et al. (2012) used this data to accurately recover the observed galaxy number counts in the 0.45–4.5 μm range. This therefore assumes only the existence of populations now observed out to $z \sim 2$–8 and magnitudes as faint as $m_{AB} \sim 23$–26; additional populations, such as the hypothetical galaxies with first stars, would then exist at still earlier times and have much fainter fluxes.

In the rest-frame UV to near-IR, the LF is well described by the conventional Schechter parameterization whereas at mid-IR wavelengths, the LF seems to be better described by a broken power-law or a double-exponential profile. Regardless of the functional form, the LFs can be integrated to give the comoving volume emissivity (we refer to this as the luminosity density) in the given rest-frame band

$$\epsilon_\nu(z) = \int L_\nu \phi(L_\nu, z) dL_\nu, \qquad (1)$$

where $\phi(L_\nu, z)$ is the measured LF. Each data point in Figures 1 and 2 represents the luminosity density given by the authors along with 1σ error bars (for references, see Table 1 in Helgason et al. (2012)). In the cases where this value is not given explicitly in the original papers, we have integrated the best-fit

parameterized LF to obtain ϵ_ν and have estimated the errors from the distribution of all of the values of ϵ_ν allowed within the 1σ solutions of the individual fit parameters. However, mutual comparison of uncertainties among the many different studies is not very meaningful since some authors include various effects in addition to the statistical errors from the method of LF estimation, such as cosmic variance, k-corrections, incompleteness, and photometric system. Here, we have chosen to maximize our wavelength and redshift coverage by letting all available measurements contribute to our fitted evolution regardless of the error treatment. In the cases where the median redshift of the sample is not explicitly given, we have placed the measurements at the midpoint of the redshift bin. Our wavelength interval is sampled at the rest-frame bands shown in the panels of Figures 1 and 2 where most of the LFs have been measured. The offsets from these defined wavelengths due to filter variations (e.g., Sloan Digital Sky Survey u' and Johnson U) are small enough to be neglected.

Motivated by the fitting formulae in Helgason et al. (2012), which we found to be reliable over a wide range of wavelengths, we consider the following three parameter fits for the evolution of the luminosity density

$$\epsilon_\nu(z) = a_\lambda (1 + (z - z_0))^{b_\lambda} \exp\left(-c_\lambda(z - z_0)\right), \qquad (2)$$

where we fix $z_0 = 0.8$. Although not restricted to Schechter LFs, this functional form for $\epsilon_\nu(z)$ is nevertheless equivalent to the underlying Schechter parameters evolving as $L^\star \propto (1 + (z - z_0))^{b_\lambda}$ and $\phi^\star \propto \exp(-c_\lambda(z - z_0))$ with a constant faint-end slope. Interpolating the rest-frame data between our 18 reference bands defines the rest-frame emissivity spectrum at any given epoch. We apply a cutoff to the spectrum above the Lyman limit, $E_{cutoff} = 13.6$ eV, corresponding to efficient absorption of ionizing photons by hydrogen in the local environments. At all lower energies, the universe is assumed to be completely
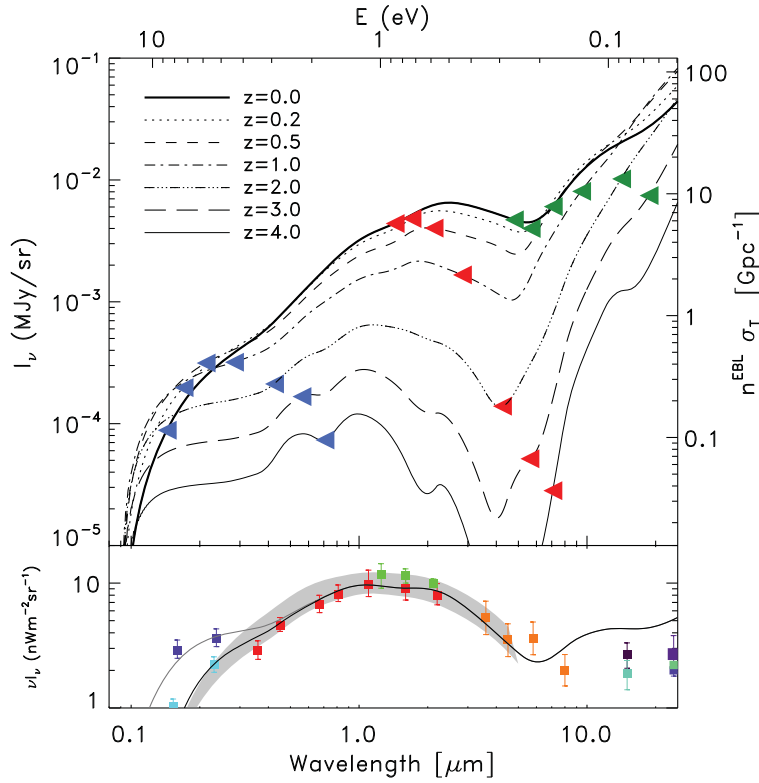
Figure 3. Upper panel: the evolving EBL resulting from our empirical reconstruction. The different lines illustrate the buildup of EBL with cosmic time leading to the present day levels (thick solid curve). We display the evolving EBL in comoving coordinates, i.e., without the expansion factor $(1+z)^3$ for better mutual comparison. The left pointing triangles show the EBL threshold energy needed to interact with an observed 30 GeV photon (blue), 300 GeV (red), and 1 TeV (green) originating at the redshifts shown. Lower panel: our reconstructed EBL compared to integrated counts in the literature along with the region bound by the upper/lower faint-end scenarios in Helgason et al. (2012) (shaded). The black and gray lines represent the case of $E_{cutoff} = 10.2$ eV and 13.6 eV, respectively. The counts data are from Gardner et al. (2000; purple), Xu et al. (2005; cyan), Madau & Pazzetti (2000; red), Keenan et al. (2010; green), Fazio et al. (2004; orange), Hopwood et al. (2010; cyan), Metcalfe et al. (2003; black), Papovich et al. (2004; deep purple), Béthermin et al. (2010; light green), Chary et al. (2004; blue).
(A color version of this figure is available in the online journal.)

transparent to background photons. The integrated light from galaxies seen today is (e.g., Peebles 1971)

$$\nu I_\nu = \frac{c}{4\pi} \int_0^\infty \nu' \epsilon_{\nu'}(z) \left| \frac{dt}{dz} \right| \frac{dz}{(1+z)}, \qquad (3)$$

where $\nu' = \nu(1+z)$ is the rest-frame frequency and

$$\left| \frac{dt}{dz} \right| = \frac{1}{H_0(1+z)\sqrt{(1+z)^3\Omega_m + \Omega_\Lambda}}. \qquad (4)$$

In Helgason et al. (2012) we considered two limiting cases for the evolution of the faint-end of the LF and showed that the distribution of galaxies from LF data, when projected onto the sky, accurately recovered the observed galaxy counts across the optical and near-infrared. The flux from the integrated counts is displayed as shaded regions in the lower panel of Figure 3 along with our empirically determined EBL (solid line) which is in good agreement with integrated counts data in the literature apart from wavelengths $\gtrsim 6$ μm where the steep evolution of the mid-IR LFs (8–24 μm) causes our EBL to be a factor of $\sim$2–3 higher than integrated counts from Chary et al. (2004), Hopwood et al. (2010), Papovich et al. (2004), and Béthermin et al. (2010). Although these authors do not claim to fully resolve the CIB at these wavelengths, the discrepancy is large enough to indicate a mismatch between number counts and mid-IR LF measurements at $z > 0.5$. This issue is apparently also encountered in galaxy evolution models;

Somerville et al. (2012) are not able to simultaneously account for the integrated counts and the bright-end of the observed LF in the 8–24 μm range using different dust templates. In fact, this is the wavelength regime where varying degrees of dust contribution and polycyclic aromatic hydrocarbon emission make the spectrum less predictable. Recent upper limits derived from a TeV source spectra also favor low levels of CIB at these wavelengths (Orr et al. 2011; Meyer et al. 2012). At this stage, one must therefore question the robustness of EBL reconstructed from LFs at $\gtrsim 8$ μm.

The UV/blue end of the EBL turns out to be sensitive to the abundance of photons with energies just below the Lyman limit, 13.6 eV. The redshifted far-UV contribution dominates the EBL below 0.5 μm due to the steep increase of the star formation rate at earlier times. For all galaxy types, there is considerable absorption in the Lyman series which we do not account for and we illustrate this dependence by considering the case where Lyman-series absorption completely suppresses the spectrum above 10.2 eV (instead of $E_{cutoff} = 13.6$ eV); shown as gray lines in Figure 3 (lower panel). We subsequently display our optical depths for the both cases which bracket the true behavior.

3. THE PHOTON–PHOTON OPTICAL DEPTH

The relevant quantity for computing the optical depth due to photon–photon interaction is the rest-frame number density of photons as a function of time and energy, $n(E, z)$. We shall refer

to the energy of a photon belonging to the EBL as E and we use $\mathcal{E}$ for the propagating γ-rays. Rest-frame quantities are denoted with a prime. At any given epoch, the photon number density (in proper coordinates) is composed both of sources emitting in the rest frame as well as the accumulated emission from earlier times

$$n(E', z) = (1+z)^3 \int_z^\infty \frac{\epsilon_{\nu'}(z')/h}{h\nu'} \frac{dt}{dz'} dz', \qquad (5)$$

where h is the Planck constant (the extra h is to convert ϵ_ν to per unit energy, $dE = hd\nu$) and $\nu' = (1+z')/(1+z)$. The condition for pair production is that the total energy in the center-of-mass frame must satisfy $\mathcal{E}'E'(1-\cos\theta) \geqslant 2(m_e c^2)^2$, where θ is the angle of incidence. This means that in order to interact with a γ-ray of energy $\mathcal{E}'$, background photons must have wavelengths of $\leqslant 1.0(\mathcal{E}'/210\,\text{GeV})\,\mu\text{m}$. The cross section for this interaction is

$$\sigma(E', \mathcal{E}', \mu)$$
$$= \frac{3\sigma_T}{16}(1-\beta^2)\left[2\beta(\beta^2-2) + (3-\beta^4)\ln\left(\frac{1+\beta}{1-\beta}\right)\right], \quad (6)$$

where

$$\beta = \sqrt{1 - \frac{2m_e^2 c^4}{E'\mathcal{E}'(1-\mu)}}, \qquad \mu = \cos\theta.$$

For the most likely angle of incidence, $\mu = 0$ (side-on), the probability for interaction is maximized at roughly four times the minimum threshold energy, $\sim 4m_e c^2/\mathcal{E}$. The optical depth encountered by a high-energy photon originating at z can be expressed in terms of its observed energy, $\mathcal{E}$, as

$$\tau_{\gamma\gamma}(\mathcal{E}, z) = c \int_0^z \frac{dt}{dz'} dz' \int_{-1}^1 (1-\mu)\frac{d\mu}{2}$$
$$\times \int_{2m_e^2 c^4/\mathcal{E}'(1-\mu)}^\infty \sigma(E', \mathcal{E}', \mu)n(E', z')dE', \quad (7)$$

where $n(E, z)$ comes from Equation (5). In Figure 4 we display the calculated optical depths as a function of observed energy for γ-rays originating at several redshifts. The optical depth roughly traces the shape of the number density of EBL photons with a sharp drop in the optical depth at the lowest energies due to the cutoff at the Lyman limit. We also show the regions encompassed by the two scenarios of the faint-end evolution from the reconstruction of Helgason et al. (2012).

4. APPLICATION TO HIGH-ENERGY OBSERVATIONS

What do these reconstructed opacities imply for observations of high-energy sources with the current instruments? Blazars and gamma-ray bursts (GRBs) are examples of high-energy extragalactic sources whose spectra is affected by the attenuation of photons in excess of $\gtrsim 10$ GeV. Two types of data sets are relevant for this discussion: space-borne *Fermi*/LAT measurements at $\lesssim 300$ GeV and ground-based telescopic measurements extending out to $\sim$TeV energies. Because extragalactic γ-ray absorption increases with both with redshift and energy, the EBL can be constrained based on the highest energy photons observed from a source provided the redshift is known (Abdo et al. 2010). GRBs have the advantages of being observable across great distances and typically displaying harder spectra than most blazars at sub-GeV energies. Figure 3 shows that for *Fermi*-observed sources it is sufficient to use data out to
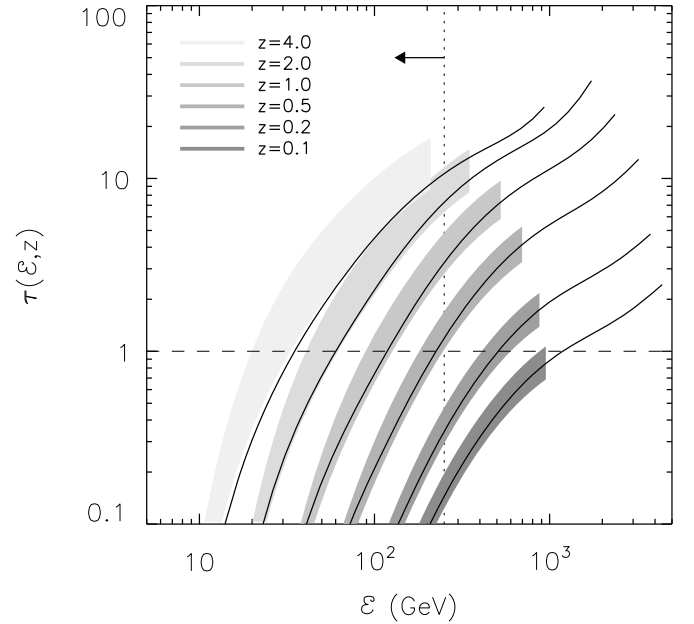

Figure 4. Solid lines show the $\gamma\gamma$ optical depth contributed by known galaxy populations assuming $E_{\text{cutoff}} = 13.6$ eV (gray curve in the lower panel of Figure 3). The curves are not drawn beyond the energy of $(m_e c^2)^2/E_{24\,\mu\text{m}}(1+z)$ as we do not consider data at $\lambda > 25\,\mu\text{m}$. The shaded regions show the boundaries of the upper/lower scenarios in the empirical reconstruction of Helgason et al. (2012) out to $4.5\,\mu\text{m}$. The dotted vertical line shows roughly the highest energy probed by *Fermi*/LAT and the dashed line shows where $\tau = 1$ for reference.

$\simeq 4.5\,\mu\text{m}$ (red symbols), whereas for TeV range observations, survey data are needed out to longer wavelengths (green symbols). Figure 4 shows the reconstructed optical depth explicitly confirming this. We now briefly discuss the implications.

Fermi/LAT detects blazars and GRBs out to energies $\sim$250–300 Gev. In Figure 5 (upper panel) we show curves of constant $\gamma\gamma$ optical depth in $\mathcal{E}$–z space and compare with the most constraining high-energy *Fermi*/LAT sources with known redshifts (taken from Abdo et al. 2010). The contours of $\tau = 1, 2, 3, 5$ correspond to probabilities of the photon being absorbed by the EBL of 63%, 86%, 95%, 99.3%, respectively. In the absence of new populations, the universe remains fairly transparent at the *Fermi*/LAT energies out to $z \sim 2$–3. Our reconstructed EBL is fully consistent with all the available LAT data and, in fact, allows for non-negligible extra levels of the CIB from new populations such as possibly have existed at higher z. As the Fermi mission progresses and Figure 5 (upper) becomes more populated at the highest energies, sources at high-z will provide better constraints for the optical/NIR EBL.

Ground-based Cherenkov telescopes have produced good quality spectra for TeV-blazars, although for sources at significantly lower redshifts than *Fermi*/LAT. If the evolving EBL is known to a good accuracy, one can deabsorb observed blazar spectra to reveal the intrinsic component, which is expected to have a power-law form, $dN/dE \propto E^{-\Gamma}$. The lower panels in Figure 5 demonstrate how our reconstructed EBL affects the spectrum of two known blazars at relatively high redshifts, both of which have been used to place upper limits on the optical/NIR EBL. Good quality spectrum of the BL Lac object 1ES 1101-232 ($z = 0.186$) has been obtained by HESS in the energy range 0.16–3.3 TeV, which for $z = 0.186$ interacts most strongly with optical and near-IR background photons (Aharonian et al. 2006). The observed spectrum is relatively hard ($\Gamma = 2.88 \pm 0.17$) and results in a best-fit intrinsic pho-
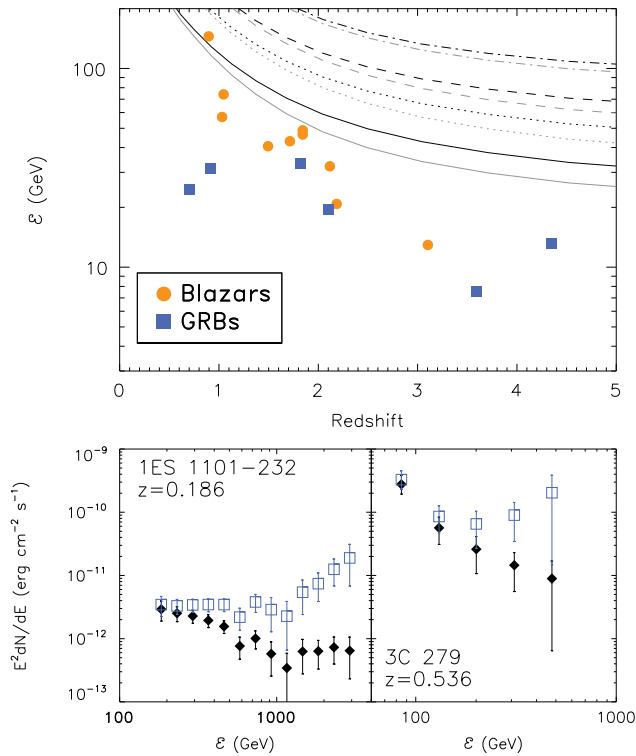
Figure 5. Upper panel: the curves show where a photon of energy $\mathcal{E}$ originating at z encounters exactly $\tau_{\gamma\gamma} = 1, 2, 3, 5$ (solid, dotted, dashed, dash-dotted, respectively). Black and gray correspond to the cases of the rest-frame spectrum cutoff energy is at 10.2 and 13.6 eV, respectively. The symbols show the highest energy photon observed in GRBs (blue squares) and a selection of the most constraining of *Fermi*/LAT blazars (orange circles) (Abdo et al. 2010; McConville et al. 2011). Lower panel: the observed energy spectrum of the sources 1ES 1101-232 ($z = 0.186$; left) and 3C 279 ($z = 0.536$; right) shown with black diamonds, and the corresponding deabsorbed data as blue squares. The deabsorbed spectra have best-fit photon indices $\Gamma_{\text{in}} = 1.49$ and $\Gamma_{\text{in}} = 2.28$, respectively, but deviate substantially from a power law at the highest energy bins.

(A color version of this figure is available in the online journal.)

ton index of $\Gamma_{\text{int}} = 1.49$ after deabsorption. For this particular source, the upturn at TeV energies is largely driven by the EBL photons at $\gtrsim 5\,\mu$m and would be less pronounced if our EBL reflected the integrated counts data in the lower panel of Figure 3. Because the EBL changes with time in both shape and amplitude, the effects on γ-ray absorption become even more prominent for more distant sources. The spectrum of the distant radio quasar 3C 279 has been captured by MAGIC during different flaring events (MAGIC Collaboration et al. 2008; Aleksić et al. 2011). The deabsorbed spectrum of 3C 279 shown in Figure 5 (lower) also deviates substantially from a simple power law in the highest energy bins, which is unlikely to be due to our near-IR background being overestimated. This behavior of the deabsorbed 3C 279 spectrum has been pointed out by Domínguez et al. (2011) who suggest either improved emission models or instrumental systematic uncertainties as potential solutions. Another possibility is that some fundamental effects are missing, such as secondary γ-rays produced along the line of sight by cosmic rays accelerated by the blazar jet (Essey & Kusenko 2010). In the absence of such secondary effects however, the universe should be completely opaque for TeV sources at $z \gtrsim 0.5$.

Upper limits for the EBL derived from TeV spectra rely on assumptions of the hardness of the intrinsic blazar spectrum. Meyer et al. (2012) derive limits for the whole range of optical

to far-IR EBL using an extensive source sample from both *Fermi*/LAT and ground-based Cherenkov telescopes. Their results allow a total integrated NIR flux (1–10 μm) of ~ 20 nWm^{-2} sr^{-1} in excess of known galaxy populations whereas there is, at most, little room for extra contribution in the mid-IR ($> 10\,\mu$m). Our LF-derived EBL is inconsistent with the lowest mid-IR limits of Orr et al. (2011).

5. SUMMARY

We have shown that it is possible to robustly reconstruct the evolving EBL in the universe using our earlier library of multiwavelength survey data now updated to extend from the UV out to the mid-IR (Helgason et al. 2012). This reconstruction uniquely defines the γ-ray opacity out to TeV energies for sources at $z \lesssim 4$ and shows that at the energy bands probed by *Fermi*/LAT, the universe is fairly transparent out to $z \sim 2$–3, unless unknown sources at high redshifts contribute nonnegligible amounts of CIB. At TeV energies, probed by groundbased telescopes, the universe becomes optically thick at $z \sim 0.5$ so any such photons associated with the sources at higher redshifts would have to be of secondary origin.

REFERENCES

Abdo, A. A., Ackermann, M., Ajello, M., et al. 2010, ApJ, 723, 1082
Aharonian, F., Akhperjanian, A. G., Bazer-Bachi, A. R., et al. 2006, Nature, 440, 1018
Aleksić, J., Antonelli, L. A., Antoranz, P., et al. 2011, A&A, 530, A4
Béthermin, M., Dole, H., Beelen, A., & Aussel, H. 2010, A&A, 512, A78
Budavári, T., Szalay, A. S., Charlot, S., et al. 2005, ApJ, 619, L31
Chary, R., Casertano, S., Dickinson, M. E., et al. 2004, ApJS, 154, 80
Domínguez, A., Serjeant, S., Negrello, M., et al. 2011, MNRAS, 410, 2556
Essey, W., & Kusenko, A. 2010, Astropart. Phys., 33, 81
Fazio, G. G., Ashby, M. L. N., Barmby, P., et al. 2004, ApJS, 154, 39
Finkelstein, S. L., Papovich, C., Salmon, B., et al. 2012, ApJ, 756, 164
Franceschini, A., Rodighiero, G., & Vaccari, M. 2008, A&A, 487, 837
Gardner, J. P., Brown, T. M., & Ferguson, H. C. 2000, ApJ, 542, 79
Gilmore, R. C. 2012, MNRAS, 420, 800
Helgason, K., Ricotti, M., & Kashlinsky, A. 2012, ApJ, 752, 113
Hopwood, R., Serjeant, S., Negrello, M., et al. 2010, ApJ, 716, L45
Kashlinsky, A. 2005a, Phys. Rep., 409, 361
Kashlinsky, A. 2005b, ApJ, 633, L5
Keenan, R. C., Trouille, L., Barger, A. J., Cowie, L. L., & Wang, W.-H. 2010, ApJS, 186, 94
Kneiske, T. M., & Dole, H. 2010, A&A, 515, A19
Le Floc'h, E., Papovich, C., Dole, H., et al. 2005, ApJ, 632, 169
Madau, P., & Pozzetti, L. 2000, MNRAS, 312, L9
MAGIC Collaboration, Albert, J., Aliu, E., et al. 2008, Science, 320, 1752
Magnelli, B., Elbaz, D., Chary, R. R., et al. 2011, A&A, 528, A35
Metcalfe, L., Kneib, J.-P., McBreen, B., et al. 2003, A&A, 407, 791
McConville, W., Ostorero, L., Moderski, R., et al. 2011, ApJ, 738, 148
Meyer, M., Raue, M., Mazin, D., & Horns, D. 2012, A&A, 542, A59
Nikishov, A. I. 1962, Sov. Phys.—JETP, 14, 393
Orr, M. R., Krennrich, F., & Dwek, E. 2011, ApJ, 733, 77
Papovich, C., Dole, H., Egami, E., et al. 2004, ApJS, 154, 70
Peebles, P. J. E. 1971, Physical Cosmology (Princeton, NJ: Princeton Univ. Press)
Pérez-González, P. G., Rieke, G. H., Egami, E., et al. 2005, ApJ, 630, 82
Rujopakarn, W., Eisenstein, D. J., Rieke, G. H., et al. 2010, ApJ, 718, 1171
Sanders, D. B., Mazzarella, J. M., Kim, D.-C., Surace, J. A., & Soifer, B. T. 2003, AJ, 126, 1607
Sawicki, M., & Thompson, D. 2006, ApJ, 648, 299
Schiminovich, D., Ilbert, O., Arnouts, S., et al. 2005, ApJ, 619, L47

Shupe, D. L., Fang, F., Hacking, P. B., & Huchra, J. P. 1998, ApJ, 501, 597
Somerville, R. S., Gilmore, R. C., Primack, J. R., & Domínguez, A. 2012, MNRAS, 423, 1992
Stecker, F. W. 1971, Cosmic Gamma Rays (NASA SP-249; Baltimore, MD: Monograph Book Corp.)
Stecker, F. W., Malkan, M. A., & Scully, S. T. 2006, ApJ, 648, 774
Stecker, F. W., Malkan, M. A., & Scully, S. T. 2012, arXiv:1205.5168

Steidel, C. C., Adelberger, K. L., Giavalisco, M., Dickinson, M., & Pettini, M. 1999, ApJ, 519, 1
Sullivan, M., Treyer, M. A., Ellis, R. S., et al. 2000, MNRAS, 312, 442
Tresse, L., Ilbert, O., Zucca, E., et al. 2007, A&A, 472, 403
Treyer, M., Wyder, T. K., Schiminovich, D., et al. 2005, ApJ, 619, L19
Xu, C., Hacking, P. B., Fang, F., et al. 1998, ApJ, 508, 576
Xu, C. K., Donas, J., Arnouts, S., et al. 2005, ApJ, 619, L11